Time-resolved x-ray imaging of a laser-induced nanoplasma and its neutral residuals

2016 New J. Phys. 18 043017

(http://iopscience.iop.org/1367-2630/18/4/043017)

New Journal of Physics
The open access journal at the forefront of physics

Deutsche Physikalische Gesellschaft DPG
IOP Institute of Physics

Published in partnership with: Deutsche Physikalische Gesellschaft and the Institute of Physics

OPEN ACCESS

RECEIVED
29 November 2015

REVISED
7 March 2016

ACCEPTED FOR PUBLICATION
22 March 2016

PUBLISHED
13 April 2016

PAPER

Time-resolved x-ray imaging of a laser-induced nanoplasma and its neutral residuals

L Flückiger[1,2], D Rupp[1], M Adolph[1], T Gorkhover[1,3], M Krikunova[1], M Müller[1], T Oelze[1], Y Ovcharenko[1,4], M Sauppe[1], S Schorb[1,3], C Bostedt[3,5], S Düsterer[6], M Harmand[6,7], H Redlin[6], R Treusch[6] and T Möller[1]

[1] Institut für Optik und Atomare Physik, Technische Universität Berlin, Hardenbergstrasse 36, D-10623 Berlin, Germany
[2] ARC Centre of Advanced Molecular Imaging, Department of Chemistry and Physics, La Trobe University, Melbourne, 3086, Australia
[3] SLAC National Accelerator Laboratory, 2575 Sand Hill Road, Menlo Park, CA 94025, USA
[4] European XFEL GmbH, Notkestraße 85, D-22607 Hamburg, Germany
[5] Argonne National Laboratory, 9700 S. Cass Avenue, Argonne, IL 60439, USA
[6] Deutsches Elektronen-Synchrotron DESY, Notkestraße 85, D-22607 Hamburg, Germany
[7] Institute of Mineralogy, Materials Physics and Cosmochemistry, 4 Place Jussieu, F-75252 Paris, France

E-mail: l.flueckiger@latrobe.edu.au

Keywords: clusters, free-electron laser, pump–probe experiment, time-resolved imaging, nanoplasma

Supplementary material for this article is available online

Abstract

The evolution of individual, large gas-phase xenon clusters, turned into a nanoplasma by a high power infrared laser pulse, is tracked from femtoseconds up to nanoseconds after laser excitation via coherent diffractive imaging, using ultra-short soft x-ray free electron laser pulses. A decline of scattering signal at high detection angles with increasing time delay indicates a softening of the cluster surface. Here we demonstrate, for the first time a representative speckle pattern of a new stage of cluster expansion for xenon clusters after a nanosecond irradiation. The analysis of the measured average speckle size and the envelope of the intensity distribution reveals a mean cluster size and length scale of internal density fluctuations. The measured diffraction patterns were reproduced by scattering simulations which assumed that the cluster expands with pronounced internal density fluctuations hundreds of picoseconds after excitation.

1. Introduction

Gas phase clusters are ideal systems to investigate the interaction between intensive light pulses and matter and in particular to follow the underlying processes of the formation and control of highly excited plasma states [1, 2]. It is of fundamental interest to understand those many-particle dynamics [3–10] but it has also interesting applications ranging from surgery [11] and controlled material processing [12] over strategies for supressing radiation damage in single-shot diffractive x-ray imaging of biomolecules [13–15] to the generation of neutron pulses by the ignition of nuclear fusion in deuterium clusters [16]. Hence for example in time-resolved measurements and calculations on clusters in intense IR pulses the significance of collective heating processes was found [17–19], which are the underlying principle for the highly efficient energy absorption of clusters in this wavelength regime [20].

With the advent of short-wavelength FELs, a new regime of intense light–matter interaction opened up, with novel opportunities for achieving high spatial and temporal resolution. The new imaging method of femtosecond coherent diffraction imaging emerged [21, 22]. For the first time it has become possible to image isolated, non-crystalline, finite targets in flight [23–25], allowing to investigate nanoparticle geometries [26, 27] and in particular ultrafast structural changes with high spatial and temporal resolution [25, 28]. Coherent diffractive imaging on single clusters has opened new avenues, especially for intense laser matter studies, because the elastic light scattering directly maps the electronic structure of the sample, i.e. the scattering response of the transient electronic structure [25] and the evolving nanoplasma after pulsed laser excitation [29].

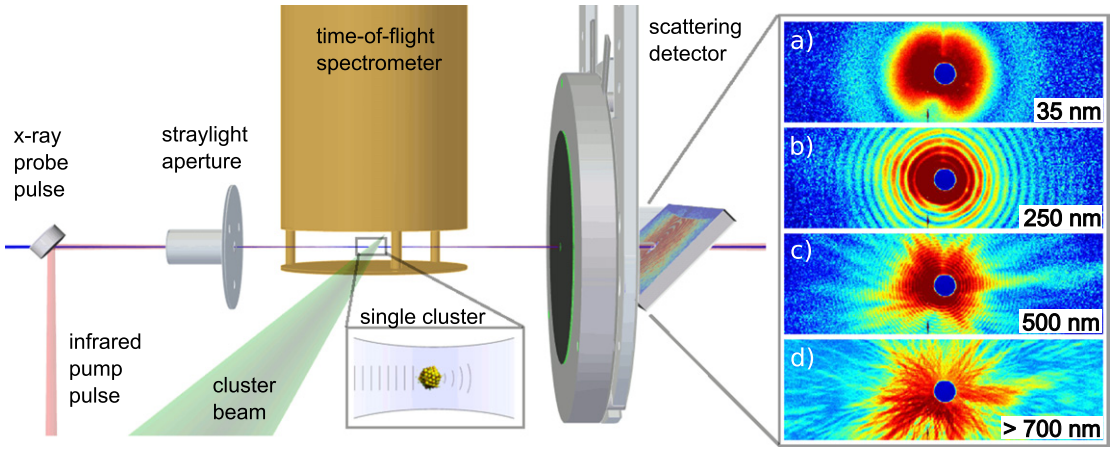

Figure 1. Schematic diagram of the experimental geometry showing the collinearly incoupled laser beams intersecting the single-cluster beam in the interaction region. An ion time-of-flight spectrometer records the ionized fragments. Scattered photons are collected with a scattering detector comprising of a multi-channel plate (MCP) and a phosphor screen. The phosphor screen is imaged with an out-of-vacuum CCD (not depicted here) via a mirror under 45°. Some artefact like dead pixels and decreased detection efficiencies appear in the recorded images which are described in more detail in the supplementary material. Diffraction patterns of individual xenon clusters imaged by soft x-ray scattering reveal the particle size and shape. With the applied source setup a wide size range was produced with the majority of clusters holding a size of 35 nm radius (a) but ranging up to extreme sizes (b)–(d), some even larger than 700 nm in radius (d).

The light induced dynamics—depending on the intensity of the light pulse—proceeds on several time scales. For strong pulses, immediately after photon absorption electrons are emitted and the particle gets ionized [4, 30]. Electron trapping by the deepening Coulomb potential [30], subsequent charge migration from the cluster surface towards its center, and the beginning of recombination take place on a femtosecond time scale [31–33]. Ion motion finally leads to sample disintegration. Its characteristics strongly depend on the power density. This process is usually completed after several picoseconds in small clusters [33–35]. For large cluster sizes the highly charged plasma evolves in shell ablation and subsequent cluster core recombination [36–39]. Theoretical work [40] and initial experiments [29, 41] provide evidence that surface softening proceeds within several hundred femtoseconds. The dynamics and the behavior of the remaining cold center part are however unknown. Theory has severe problems to model the complex dynamics up to long timescales, since they are challenging and extremely time consuming.

We performed single-shot single-cluster scattering experiments on individual large xenon clusters. By removing the averaging over cluster size and laser intensity, via sorting the single-shot images in post-analysis, the blurring of clear signatures is avoided [42–44]. In order to entirely follow the long-term expansion dynamics of the cluster, imaging experiments were pushed up to the nanosecond time scale in a pump–probe setup. The cluster expansion initiated by an ultrashort infrared (IR) pulse [45] was imaged with a soft x-ray FEL pulse from the FLASH facility at DESY [46]. With this method we were able to directly image two fundamentally different stages of cluster evolution.

- On a picosecond time scale, scattering patterns exhibit decreasing fringe signal at high scattering angles. This indicates a softening of the cluster surface while the center part stays intact.
- After a nanosecond, speckle patterns reveal the survival of the cluster core. Image analysis points towards the core remaining as diluting neutral particle with internal density modulation.

Diffraction patterns from these extreme evolution states give unprecedented access to an up-to-date unseen phase of radiation-induced cluster dynamics.

2. Experiment

A schematic diagram of the experimental geometry is presented in figure 1. Extremely large individual xenon clusters are produced in a pulsed supersonic expansion through a cooled conical nozzle (180 K, 200 μm diameter, 4° half opening angle) with 10 bar backing pressure. Production of such large particles is experimentally challenging and triggered the development of a new experimental approach for rare-gas cluster generation [47]. The source setup and valve operation scheme are described previously [47]. For imaging in

single-particle mode the cluster beam was heavily skimmed down until only one single particle was intercepted with the light pulses in the interaction region [25, 26, 43].

The FLASH free-electron laser facility delivered soft x-ray pulses with 13.6 nm wavelength and about 100 fs pulse length in single-bunch mode [46, 48]. We used the focused branch of the FLASH beamline, BL2, where the FEL power density reached peak intensities of up to 4×10^{14} W cm^{-2}. Far-field scattering patterns were recorded with the detector system described in [25] at a distance of 61.6 mm behind the interaction region, recording scattering angles up to 32°. The central part up to 4° is not detected due to a central hole in the detector setup, preventing beam damage. A gating scheme was applied to ensure that only photons were detected (see supplementary material for details). To take the flatness of the detector into account, all images were intensity corrected with a factor of $\cos(\theta)^{-3}$ [25]. From the single-pulse scattering patterns each cluster size was individually determined by fringe spacing analysis [47]. The statistical nature of the growth process results in a broad log-normal size distribution. Its maximum is identified at 35 nm radius. A representative pattern from a cluster of this size is shown in figure 1(a). Most prominent but less abundant are patterns resulting from very large clusters up to a micron in radius, shown in figures 1(b)–(d). Smaller particles are predominantly round in shape reflected by circular scattering patterns. For largest particle sizes the fine interference fringes were not resolvable with our detector setup. In line with recent findings [47] they exhibit a rough surface since they freeze out in non-spherical shapes during their growth by coagulation.

Imaging of nanoplasma evolution was established with pump–probe technique. Synchronized to the FEL pulses, 800 nm Ti:Sapphire pulses of 80 fs duration [45] were collinearly coupled into the vacuum chamber via a holey mirror (see figure 1). The IR pulses were vertically polarized and their focal power density was determined to be about 10^{14} W cm^{-2}. The IR pump-pulse focal area with a FWHM of 90 μm was overlapped with the 20 μm soft x-ray probe pulse using an in-vacuum microscope. Isochronous pulse arrival ('time zero') was established with sub ps-resolution by tracing the ion yield of the transient Xe^{3+} charge state [49] with an ion time-of-flight spectrometer. The relative timing jitter between Ti:Sa and FEL pulse was about 0.4 ps, as measured with the streak camera setup at FLASH [50]. In order to gain insight into manifold steps of the nanoplasma evolution upon IR excitation, the pump pulse arrival time was scanned in a wide range from 0.5 ps up to 1.5 ns before inception of the probe pulse, i.e. the instant of time when the particle was imaged.

The method of single-shot imaging requires a large amount of data to be collected in order to ensure meaningful statistics. Despite opening new possibilities it also demands novel filtering routines [51]. From the evolution-initiating IR pulse only a fluorescence is recorded and not a scattering pattern. Therefore, in the pump–probe experiment the initial cluster size and exposed power density is not well defined. However, the final state of the excited cluster, at probe time, is detected by the FEL pulse. A reliable filtering method was needed to make patterns of different final states comparable, despite missing knowledge of the initial state. A very basic but effective method was to filter scattering patterns with highest detector intensity. It was assumed that these images resulted from the largest clusters, as they scatter significantly stronger than smaller ones. Additionally we presume that the strong scattering intensity is an indication that the cluster was exposed to maximal FEL power densities. There the higher number of impinging photons should result in a larger number of scattered photons. Note that the current detector system used was not a single photon counter detector and that the photon signal was converted to electronic and optical signal before data storage [25]. Therefore no absolute values can be given for the detector intensity. Nevertheless, sorting of *relative diffraction pattern intensities* makes a reliable filter as shown in earlier experiments [25].

3. Results

The analysis of laser induced nanoplasma evolution is divided in two phases to account for the different expansion processes occurring during a nanosecond time interval. First the evolution of the outer cluster shell is investigated (section 3.1) and subsequently the whereabouts of the center part are examined in detail (section 3.2).

3.1. Surface ablation

In this section the gradual change in scattering patterns with cluster evolution on a picosecond time scale is analyzed. Figure 2 depicts snapshots of different individual xenon clusters recorded without pre-irradiation (a) and at various delay times after sample excitation with the IR pump pulse (b)–(e). As mentioned above, the initial cluster state upon IR laser excitation cannot be directly extracted from the recorded images. To eliminate the influence of particle size and focal position, for each delay time, the scattering pattern with highest detector intensity is chosen. It is assumed that these patterns result from the largest xenon clusters (700–1000 nm radius) in the size distribution intercepted at the central FEL focus position. These large clusters grow by coagulation of smaller particles and can freeze out in intermediate states resulting in mostly spherical particles with grainy

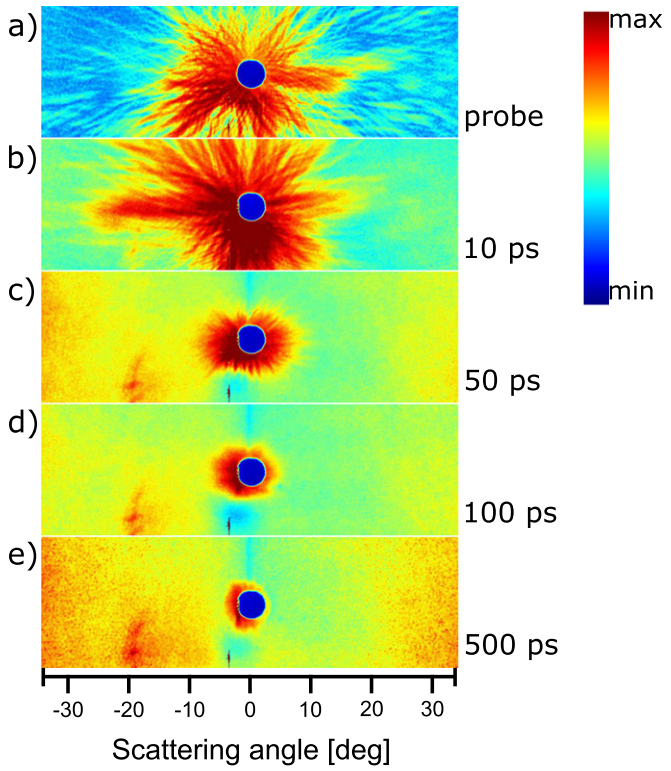

Figure 2. Scattering patterns from xenon clusters imaged with the soft x-ray pulse without pre-irradiation (a), and at several delay times after the IR pulse excitation (b)–(e). Each pattern is the most intense out of all images recorded at the indicated delay time. This selection is based on the assumption that sorting for intensity filters the largest and best hit particles and thus comparable initial conditions. Exclusive probe pulse imaging (a) shows an intact particle with radius larger than 700 nm. In pump–probe configuration (b)–(e) with increasing delay time the low frequency information is blurred revealing proceeding particle surface ablation. The bright diffuse spot at around -20° on the left side of the scattering patterns is an artifact originating from reflections of the IR laser on the out-of-vacuum CCD camera (see supplementary material for details).

substructure [47]. These hailstone-shaped particles lead to characteristic fringe patterns in the diffraction images (figure 2(a)). At early delays (figure 2(b)) the fringe structure is visible over a wide angle range, showing that conjecturably the grainy substructure on the particle surface is still intact after 10 ps. Immediately visible from comparison of figures 2(b)–(e) is the loss of fine structure at higher scattering angles with proceeding delay. From 50 ps onwards (figure 2(c)) it gradually blurs and vanishes starting from the outer detector region towards the center. At the same time a background signal arises with stronger contribution at high angles.

For a qualitative analysis of the particle evolution in time, the recorded scattering patterns depicted in figure 2 are azimuthally integrated and their profiles are plotted in figure 3(a). The fine interference rings cannot be resolved due to the detector resolution; therefore the size of the clusters cannot be extracted. However the cluster evolution can be extracted from the changing of the intensity envelopes.

With increasing delay time a background signal arises, especially at high scattering angles. Its origin is unknown but might result from fluorescence and inelastic scattering. In the literature an increase in background signal at high scattering angles due to inelastic scattering was predicted by theoretical models [40]. A similar appearance in photon intensity at large angles was reported in an earlier dynamic imaging experiment [52].

The key observation in the here presented patterns is that the envelope slopes of the scattering signal at small angles get steeper with increased delay time, which we attribute to coherent diffraction signal from the evolving cluster. This observation is also found in a recent experiment studying a different size regime of xenon clusters [29] and is well explained by theoretical calculations on hydrogen clusters [40]. In both works the intensity lowering of higher order fringe maxima in scattering patterns from a spherical cluster is attributed to surface ablation.

We conducted comparative calculations following the theory in [40] to understand the correlation between surface ablation and decrease of fringe intensity in much more detail. They show that only a few percent of the cluster need to melt off to result in such a steepening of the radial profiles. To find a suitable choice for the parameters in the calculation is not unambiguous since the initial radius of the cluster is unknown. The following assumptions were made. To mimic the cluster shapes at several time steps after IR irradiation, various electron density distributions with increasingly softened surface and corresponding shrinking full-density core

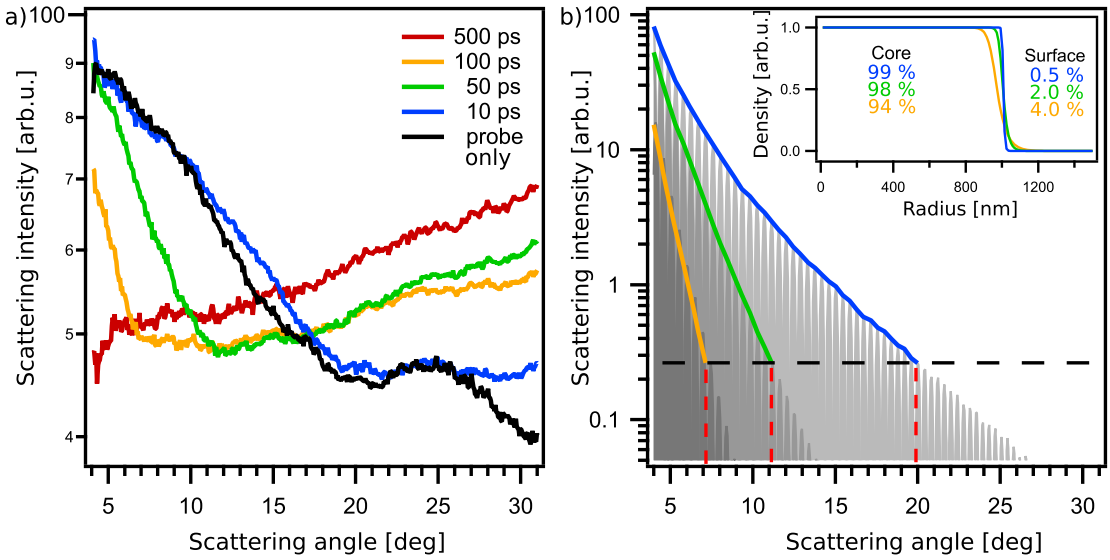

Figure 3. (a) Azimuthally integrated scattering pattern profiles reveal an increase in envelope steepness with delay time. Additionally the scattered background level increases with delay time especially at high angles. (b) Inset: several cluster electron density distributions for particles with increasingly softened surface. Calculated increasing shell ablation results in decreasing core radius since the overall particle volume is kept constant. (b) Full image: profiles of 2D FFTs from the projected densities show the correlation between shell ablation and scattering signal decrease at high scattering angles. Scattering fringes are plotted in gray and envelopes are highlighted in color. With evolving surface softening the scattering envelope increases in steepness.

are calculated and displayed in the inset of figure 3(b). For the calculation of the electron density distribution an analytic expression proposed by MicPIC theory for nanoplasmas in hydrodynamic expansion [40] was employed:

$$n(r) = \frac{n_{\mathrm{Core}}}{\left[\exp\left(\frac{r - r_{\mathrm{Core}}}{ds}\right) + 1\right]^{s}}, \tag{1}$$

where n_{Core} is the core density, r_{Core} the core radius, d the decay length of the melting surface, and s an additional sharpness factor. In a simplified approach scattering profiles were simulated by 2D fast Fourier transforms (FFTs) of the electron density distribution projected onto the scattering plane and presented in figure[8] 3(b). No absolute photon intensities are measurable with this detector setup. Thus, to be able to compare theory and experiment, scattering slopes are not directly compared, but a rather different approach is used: an intensity threshold was set where the recorded scattering signal merges with background noise, as indicated by the black dashed lines in figure 3(b). The scattering angle, at which envelope and threshold level cross (indicated by red dashed lines in figure 3(b)), was used as reference point to find the matching density profiles. The slope of a scattering envelope from a spherical object is independent on the particle size [53]. Therefore any arbitrary initial radius is applicable to study the intensity envelope changes. As discussed above, the initial cluster size cannot be extracted from the recorded images, but since profiles are filtered on brightest image presumably resulting from largest clusters in the beam, an initial radius of 1000 nm was assumed.

Three electron density distributions with increasing surface ablation and, correspondingly, with the reduced core-size were calculated (inset in figure 3(b)). Thereby the overall particle volume was kept constant, e.g. the integral under the outline was always kept the same. With increasing surface melt-off and decreasing core the scattering profiles become steeper. From the profile simulated for the scattering pattern recorded 100 ps after IR excitation (orange profile), it becomes evident that only a minor part of the core needs to melt off before the characteristic scattering fringes of large clusters are almost completely vanished. The absolute values in this calculation are not viable but the simulation clearly show that in our setup the scattering patterns vanish much faster than the clusters themselves.

Our findings confirm earlier studies performed with ion spectroscopy on large argon clusters in IR light [36]. It showed that for moderate IR intensities (10^{14} W cm^{-2}) the cluster is skinned with the layer of certain thickness depending on the laser power. A recent study on large xenon clusters in soft x-ray light indicates a similar behavior [39]. A thin, highly charged cluster shell expands upon hydrodynamic pressure of the nanoplasma electron cloud. The remaining core recombines to full neutrality [39] after electrons migrate to the energetically preferred cluster center [13]. Here we show that these disintegration dynamics of such large xenon clusters can

[8] In this approximation absorption effects are neglected.

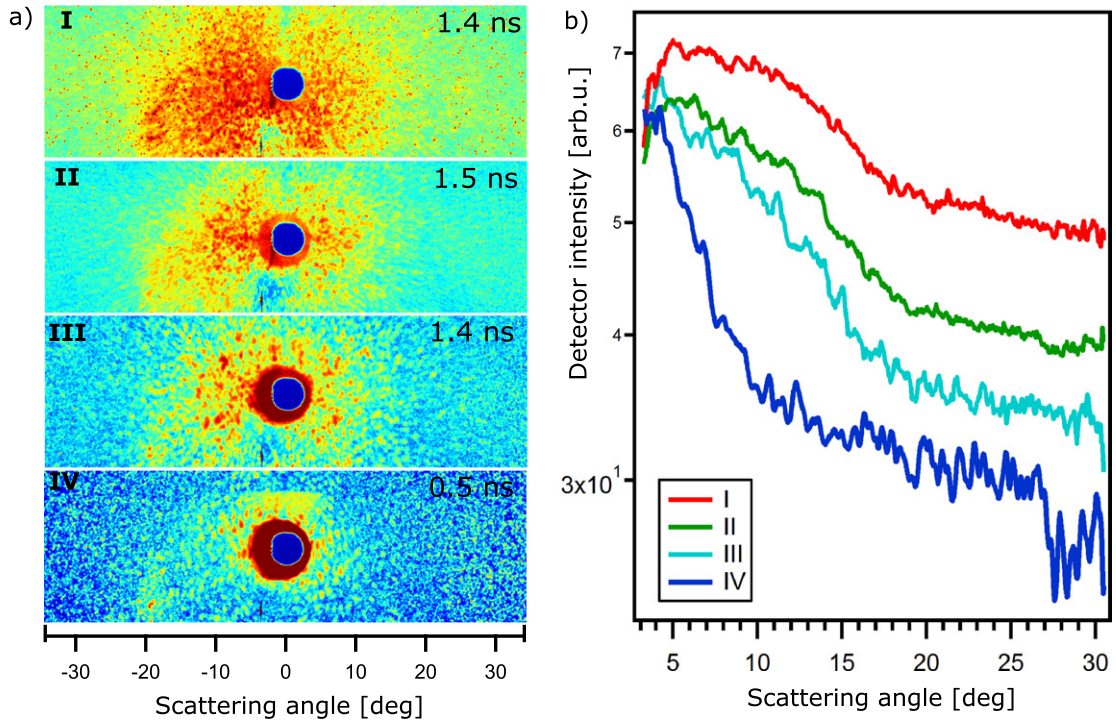

Figure 4. (a) Characteristic speckle patterns, recorded upon soft x-ray irradiation of single clusters 1.5 ns after IR laser excitation. (b) Corresponding azimuthally integrated scattering intensities show a modulation in the amplitude envelope with change of slope at around 20°scattering angle and lower.

be directly imaged. From the above simulation we can estimate that after 100 ps a substantial part of the cluster core can still be intact, even though the coherent scattering signal has already vanished towards small scattering angles and is overlaying with background signal, especially at high detection angles. The further fate of the recombined inner part of the cluster [39] however, is fully unknown. The disintegration of the central part of the cluster is subject of the next section.

3.2. Core disintegration

3.2.1. Measured speckle patterns

On a long timescale, from 500 ps on, a novel kind of pattern shows up as presented in figure 4(a). These speckle patterns from fragmenting xenon clusters were to our knowledge never detected before from atomic clusters but are mainly known from imaging of colloid systems [28, 54, 55]. All three patterns exhibit a characteristic speckle distribution with distinct speckle size and intensity. As these images are low in overall scattering intensity (compare with figure 2(e)), they probably result from small clusters. Note that the cluster size distribution is broad with a maximum of 35 nm radius, as stated in the experimental section.

Figure 4(b) presents the azimuthally integrated intensities of the speckle patterns in figure 4(a). A change in the slope of the intensity envelope is seen in the experimental scattering profiles around 20°.

A detailed analysis of the speckle pattern can provide information on the particle shape [56] and density [57]. In the case of dense spherical objects the analysis of the intensity profiles would give information of different object properties. in full analogy, the ring spacing corresponds to the particle size, while the intensity envelope depends on the materials refractive index, which is coupled to the electron density [53]. In a similar way, the mean size of speckles is inversely proportional to the average radius of the overall object [56, 58] and the slope of a speckle distribution is correlated with the average characteristic length scale of the internal structure which induces scattering [57].

Structural information from scattering patterns can in principle be gained by reconstruction with phase retrieval methods [59]. However, for disintegrating targets this procedure is challenging, especially if important information at small scattering angles is missing due to the hole in the scattering detector. Recent experiments demonstrated that reconstruction gets extremely difficult with increasing loss of detailed structure in the sample [52]. Instead of phase retrieval methods we therefore performed simulations which can provide new insight into the main characteristic of the sample disintegration. We start with a systematically analysis to understand main features of speckle patterns (section 3.2.2) and as a second step try to modulate measured scattering patterns in a simplified model (section 3.2.3).

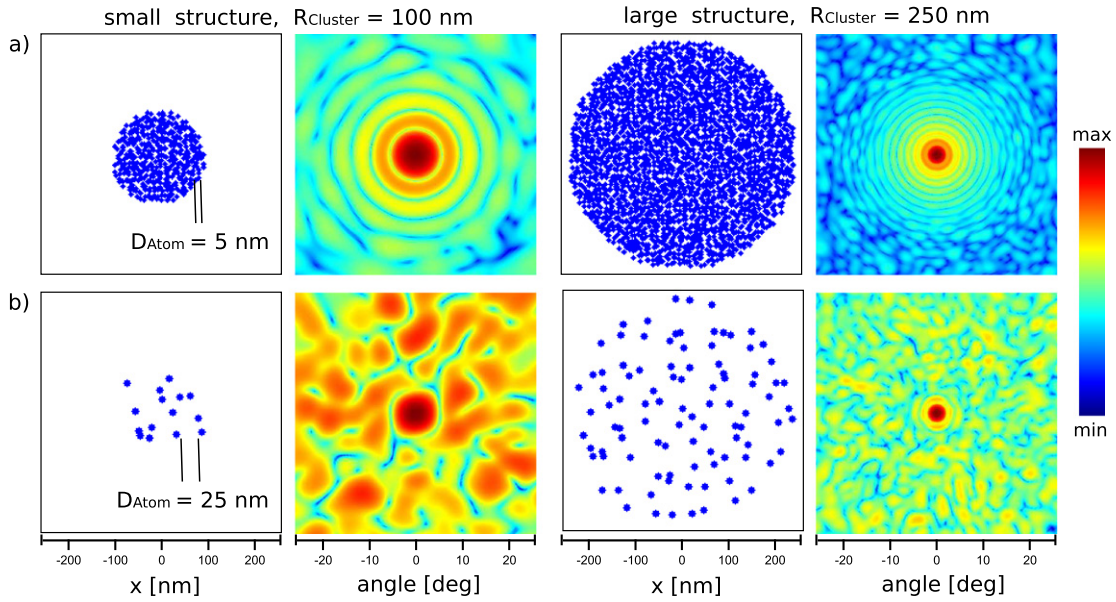

Figure 5. Emergence of speckle patterns: central cuts through modeled cluster geometries of small (left half: $R = 100$ nm) and large (right half: $R = 250$ nm) particles and corresponding SAXS simulations. For better visibility the pattern intensities are normalized to their respective maximum value. Therefore absolute values for different simulations are not comparable in this depiction. (a) A dense particle with smooth surface gives ring-patterns known from Mie theory. (b) For a dilute particle with rough surface the scattering images contains speckles with constant intensity distribution.

3.2.2. Method: small-angle x-ray scattering (SAXS) simulations

We systematically computed scattering patterns from model clusters with SAXS simulations in numerical scalar approach [60]. In a first step, scattering from a sphere with amorphously distributed point-scatterers has been investigated. In a second step, the cluster has been further divided into sub-spheres to account for internal density fluctuations. By tuning the parameters of the overall cluster size, atomic distance, sub-sphere size, and their spacing, the response on the scattering pattern are systematically studied and presented in figures 5 and 6.

Scattering from a 'gas ball', with in average equal atom spacing significantly smaller than the impinging laser wavelength, results in ring patterns (figure 5(a)). The fringe spacing is inversely proportional to the overall particle radius R_{Cluster}, as evident from Fraunhofer diffraction. Please note that absolute scattering intensities scale with the number of scatterers. For better visibility all simulated scattering patterns are normalized to their respective maximum intensity and absolute values are not directly comparable. With increase in distance between the point scatterers D_{Atom} (from figures 5(a) to (b)) ring patterns break up and transform into speckles, gradually evolving from large to small scattering angles. This is equivalent to the transition from a homogeneous to an inhomogeneous sample, leading at the same time to an increase in surface roughness. Analogous to interference rings from dense objects the speckle size decreases with growing sphere size (see figure 5(b) top to bottom). The *average particle radius* can be determined from the *mean speckle size* by [56, 58]

$$R_{\mathrm{Cluster}} = \frac{\lambda \cdot L}{\pi \cdot R_{\mathrm{Speckle}}} \tag{2}$$

with λ the impinging wavelength, L the distance between detector and interaction region, and R_{Speckle} the mean speckle radius on the detector (the detector pixel size multiplied by half the number of pixel length an average speckle occupies). Note that if the distance between the atoms becomes larger than the transversal coherence length of the laser beam, speckles can not be resolved [61].

Fluctuations in the particle density have been implemented in the simulation by modeling spherical sub-clusters of point-scatterers with radius R_{Sub} and distance between their center points D_{Sub} (figures 6(a) and (b)). They lead to modulations in the diffraction amplitude envelope, as indicated by red dashed lines in figures 6(a) and (b). From the Airy pattern formula [62]

$$R_{\mathrm{Sub}} = \frac{1.22 \cdot \lambda}{2 \cdot \sin(\theta_{\mathrm{min}})} \tag{3}$$

the *average fluctuation range* is inversely correlated to the *angle of the first order minimum* θ_{min} of the scattering envelope modulation. As simulations emphasize, with increasing sub-cluster radius the modulation minimum shifts towards smaller scattering angles (from figures 6(a) to (b)). Note that the speckle size is unaffected by the density modulation (compare figures 5 and 6).

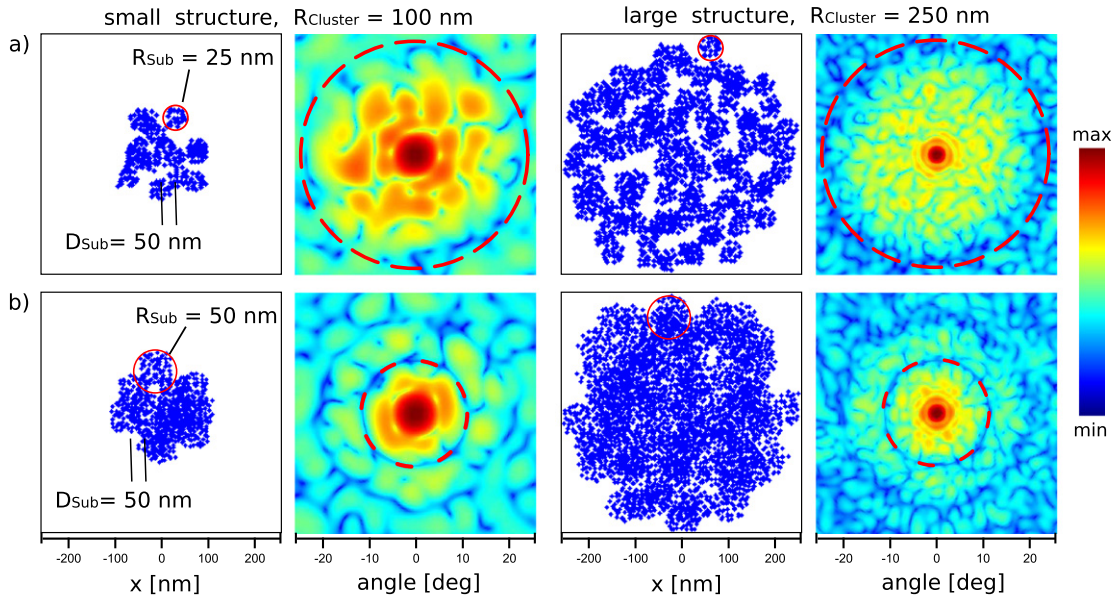

Figure 6. Emergence of intensity modulation: central cuts through modeled cluster geometries of small (left half: $R = 100$ nm) and large (right half: $R = 250$ nm) particles and corresponding SAXS simulations. Pattern intensities are normed to their respective maximum value. (a) Internal density modulations result in a modulation of the amplitude envelope visible as ring-shaped superstructure at high angle, indicated by red dashed circles. (b) With increasing range of density modulation the envelope minima shift to smaller angles. For the simulations in c and d the atomic distance is kept constant at 5 nm.

3.2.3. Cluster evolution determined from speckle analysis

The size of the cluster debris, at a nanosecond after IR irradiation, can be characterized with the measured speckle patterns by the dependencies stated above. Exemplifying we discuss pattern II and IV in figure 4(a). The mean speckle size can be deduced with several image analysis methods. Here we performed the normalized autocovariance of the speckle pattern [63]. The width of its intensity profile at $1/e^2$ of the maximum intensity provides a reasonable measurement of the average width of a speckle [63]. In our experimental setup with wavelength $\lambda = 13.6$ nm and detector distance $L = 61.6$ mm, the average speckle in pattern II covers in length 8.06 pixels of the detector, related to a mean speckle radius of $R_{\mathrm{Speckle}} = 0.28$ mm due to a detector pixel size of $p = 0.069$ mm. This corresponds to a cluster radius of about 950 nm (see equation (2)). For pattern IV the mean speckle radius is 0.33 mm (9.61 pixel) analogous to a mean cluster radius of about 800 nm. A change of slope in the amplitude envelope is found at approximately 20°(see envelope II in figure 4(b)). This corresponds to about 25 nm range in density fluctuations, which is mimicked by sub-cluster radius in this simulation. For pattern IV it is challenging to determine a minimum due to the low schattering signal. However, a simulation with $R_{\mathrm{Sub}} = (52 \pm 30)$ nm seems to fit best.

The overall particle density determined by the atomic and sub-cluster distance, cannot be directly extracted from the measured pattern. This is because the important central part of the pattern up to 4° is missing, due to the detector center hole and stray light out of the beamline, as introduced in the experimental section and encircled by a red ring in figures 7(a) and (b). For small scattering vector values, e.g. towards the central part, the particle looks dense. For larger angles the scattering signal is sensitive to the distance of the scatterers. Therefore the scattering angle of the transition between ring pattern and speckle structure is correlated to the density of the cluster (figure 5(a)). This enables us to give a lower limit of the particle density in the cluster. A model cluster with a distance of 50 nm between sub-sphere centers and 4 nm distance between atoms within the sub-spheres fits a transition from ring to speckle pattern below 4° angle. For pattern IV a model with $D_{\mathrm{Atom}} = 10$ nm and $D_{\mathrm{Sub}} = 104$ nm has been used.

Figure 7(b) shows a suitable simulation with these values, of a $R_{\mathrm{Sphere}} = 950$ nm cluster, divided in sub-spheres of in average $R_{\mathrm{Sub}} = 25$ nm. To make the model more realistic, we included a distribution of density modulation length. Therefore, the sub-cluster size has been distributed between 10 and 40 nm radius (figure 7(c)) which results in a less pronounced amplitude modulation (figure 7(d)). Azimuthally integrated intensity profiles reveal that the slope can be reproduced properly (figure 7(d)). The method of SAXS simulations on clusters with internal density fluctuations shows that even though the complexity of the speckle patterns makes an exact particle characterization impossible, the characteristic length scales of the evolving cluster can be extracted.

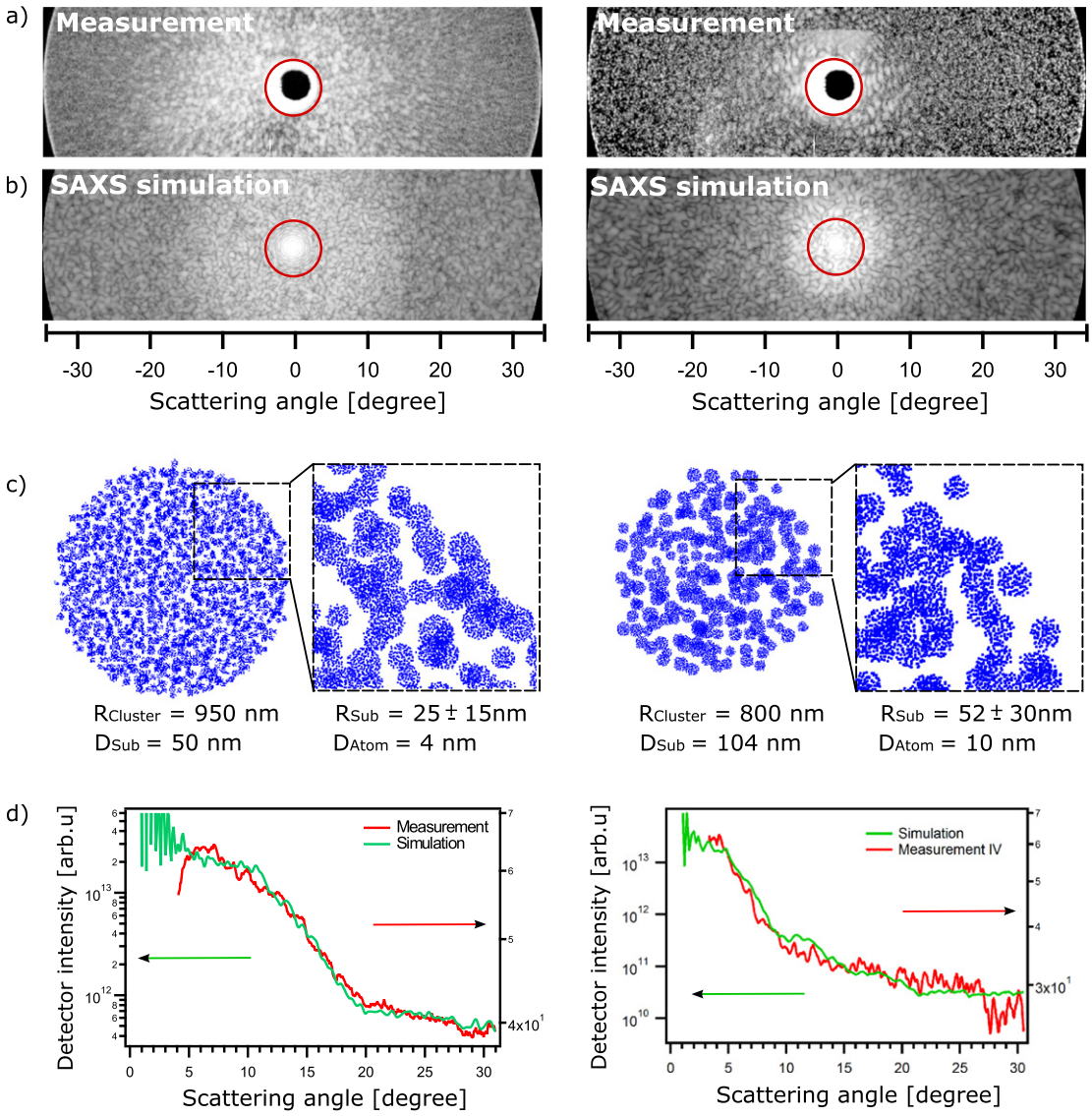

Figure 7. (a) Typical speckle diffraction pattern recorded 1.4 ns (II) and 0.5 ns (IV) after IR laser impingement. (b) Simulated pattern calculated in scalar numerical small angle x-ray scattering approach from a $R_{\mathrm{Cluster}} = 950$ nm dilute gas ball with internal density fluctuations on a size range of $R_{\mathrm{Sub}} = (25 \pm 15)$ nm and a cluster with $R_{\mathrm{Cluster}} = 800$ nm and $R_{\mathrm{Sub}} = (52 \pm 30)$ nm. (c) Visualization of the model clusters used to calculate (b). Atomic distances are set to $D_{\mathrm{Atom}} = 4$ nm and sub-cluster distances to $D_{\mathrm{Sub}} = 50$ nm, respectively $D_{\mathrm{Atom}} = 10$ nm and $D_{\mathrm{Sub}} = 104$ nm. (d) Radial profiles of measured and simulated data show the elaborateness of input values. The intensity scale for measured and simulated data varies due to the ambiguous linearity of the scattering detector.

4. Conclusion

We explored cluster evolution by snapshotting time-slices of laser induced disintegration in pump–probe configuration, pushing to extreme time regimes from several pico- up to 1.5 ns. After initiation of the expansion with an intense IR laser pulse, xenon clusters in the size range of several ten to hundred nanometers in radius were imaged with a soft-x-ray FEL pulse in single-shot single-particle mode. We identified two different kinds of scattering patterns on different time scales: fringe patterns, where the scattering signal vanishes at high scattering angles with increasing delay time within tens of picoseconds, as well as speckle patterns, which appear from 500 picoseconds onwards.

We attribute these two types of patterns to different stages of the expansion:

- Following strong particle excitation and subsequent electron trapping in the deepening Coulomb potential a quasi-neutral nanoplasma is formed. Its surface ions undergo hydrodynamic expansion due to the pressure of the plasma electrons [38]. The expansion evolves on a picosecond timescale layer-wise from the outside towards the cluster center. This surface softening is mirrored by a decrease in scattering signal at high scattering angles (see also [29, 40]).

- Meanwhile the majority of excited electrons recombines and consequently the expansion driven by plasma electrons finally stops. The remaining neutral cluster core stays in the interaction region up to nanoseconds. Its density decreases slowly and density fluctuations occur, leading to speckle patterns with intensity modulations.

We show that simple image analysis of the recorded speckle patterns has the potential to determine the overall size and internal density fluctuation range of the examined object. Our findings from dynamic diffraction imaging extend the picture of laser–matter interaction into the nanosecond time scale, where we identifed structural signatures up to date not explored in homogeneous clusters.

Acknowledgments

The authors like to thank the DESY staff for their outstanding support during FLASH beamtime as well as Thomas Fennel, Christian Peltz and Ivan Vartanyants for fruitful discussions. Financial support by the BMBF grand 05K10KT2 is kindly acknowledged.

References

[1] Fennel T, Meiwes-Broer K H, Tiggesbäumker J, Reinhard P G, Dinh P M and Suraud E 2010 *Rev. Mod. Phys.* **82** 1793–842
[2] Saalmann U, Siedschlag C and Rost J M 2006 *J. Phys. B: At. Mol. Opt. Phys.* **39** R39–77
[3] Snyder E, Buzza S and Castleman A 1996 *Phys. Rev. Lett.* **77** 3347–50
[4] Wabnitz H *et al* 2002 *Nature* **420** 482–5
[5] Laarmann T, de Castro A, Gürtler P, Laasch W, Schulz J, Wabnitz H and Möller T 2004 *Phys. Rev. Lett.* **92** 143401
[6] Iwayama H *et al* 2009 *J. Phys. B: At. Mol. Opt. Phys.* **42** 134019
[7] Varin C, Peltz C, Brabec T and Fennel T 2012 *Phys. Rev. Lett.* **108** 175007
[8] Ziaja B, Chapman H N, Fäustlin R, Hau-Riege S, Jurek Z, Martin A V, Toleikis S, Wang F, Weckert E and Santra R 2012 *New J. Phys.* **14** 115015
[9] Schütte B, Arbeiter M, Fennel T, Vrakking M J J and Rouzée A 2014 *Phys. Rev. Lett.* **112** 073003
[10] Müller M *et al* 2015 *J. Phys. B: At. Mol. Opt. Phys.* **48** 174002
[11] König K, Riemann I, Fischer P and Halbhuber K J 1999 *Cell. Mol. Biol.* **45** 195–201
[12] Englert L, Wollenhaupt M, Haag L, Sarpe-Tudoran C, Rethfeld B and Baumert T 2008 *Appl. Phys.* A **92** 749–53
[13] Hoener M, Bostedt C, Thomas H, Landt L, Eremina E, Wabnitz H, Laarmann T, Treusch R, Castro A R B D and Möller T 2008 *J. Phys. B: At. Mol. Opt. Phys.* **41** 181001
[14] Iwan B *et al* 2012 *Phys. Rev.* A **86** 033201
[15] Schorb S *et al* 2012 *Phys. Rev. Lett.* **108** 233401
[16] Ditmire T, Zweiback J, Yanovsky V P, Cowan T E and Hays G 1999 *Nature* **398** 489–92
[17] Köller L, Schumacher M, Köhn J, Teuber S, Tiggesbäumker J and Meiwes-Broer K H 1999 *Phys. Rev. Lett.* **82** 3783–6
[18] Zweiback J, Ditmire T and Perry M 1999 *Phys. Rev.* A **59** 3166–9
[19] Saalmann U and Rost J M 2003 *Phys. Rev. Lett.* **91** 223401
[20] Ditmire T, Donnelly T, Rubenchik A, Falcone R and Perry M 1996 *Phys. Rev.* A **53** 3379–402
[21] Chapman H N *et al* 2006 *Nat. Phys.* **2** 839–43
[22] Neutze R, Wouts R, van der Spoel D, Weckert E and Hajdu J 2000 *Nature* **406** 752–7
[23] Bogan M J *et al* 2008 *Nano Lett.* **8** 310–6
[24] Bostedt C, Adolph M, Eremina E, Hoener M, Rupp D, Schorb S, Thomas H, de Castro a R B and Möller T 2010 *J. Phys. B: At. Mol. Opt. Phys.* **43** 194011
[25] Bostedt C *et al* 2012 *Phys. Rev. Lett.* **108** 093401
[26] Rupp D *et al* 2012 *New J. Phys.* **14** 055016
[27] Barke I *et al* 2015 *Nat. Commun.* **6** 6187
[28] Bogan M J *et al* 2010 *Aerosol Sci. Technol.* **44** i–vi
[29] Gorkhover T *et al* 2016 *Nat. Photon.* **10** 93–7
[30] Bostedt C *et al* 2008 *Phys. Rev. Lett.* **100** 133401
[31] Bostedt C, Thomas H, Hoener M, Möller T, Saalmann U, Georgescu I, Gnodtke C and Rost J M 2010 *New J. Phys.* **12** 083004
[32] Saalmann U 2010 *J. Phys. B: At. Mol. Opt. Phys.* **43** 194012
[33] Krikunova M *et al* 2012 *J. Phys. B: At. Mol. Opt. Phys.* **45** 105101
[34] Krainov V and Smirnov M 2002 *Phys. Rep.* **370** 237–331
[35] Arbeiter M, Peltz C and Fennel T 2014 *Phys. Rev.* A **89** 043428
[36] Sakabe S, Shirai K, Hashida M, Shimizu S and Masuno S 2006 *Phys. Rev.* A **74** 043205
[37] Thomas H, Bostedt C, Hoener M, Eremina E, Wabnitz H, Laarmann T, Plönjes E, Treusch R, De Castro A R B and Möller T 2009 *J. Phys. B: At. Mol. Opt. Phys.* **42** 134018
[38] Arbeiter M and Fennel T 2011 *New J. Phys.* **13** 053022
[39] Rupp D *et al Phys. Rev. Lett.* submitted
[40] Peltz C, Varin C, Brabec T and Fennel T 2014 *Phys. Rev. Lett.* **113** 133401
[41] Hau-Riege S P *et al* 2010 *Phys. Rev. Lett.* **104** 064801
[42] Islam M, Saalmann U and Rost J 2006 *Phys. Rev.* A **73** 041201 (R)
[43] Gorkhover T *et al* 2012 *Phys. Rev. Lett.* **108** 245005
[44] Hickstein D D *et al* 2014 *Phys. Rev. Lett.* **112** 115004
[45] Redlin H, Al-Shemmary A, Azima A, Stojanovic N, Tavella F, Will I and Düsterer S 2011 *Nucl. Instrum. Methods Phys. Res.* A **635** S88–93

[46] Tiedtke K et al 2009 New J. Phys. 11 023029
[47] Rupp D et al 2014 J. Chem. Phys. 141 044306
[48] Ackermann W et al 2007 Nat. Photon. 1 336–42
[49] Krikunova M et al 2009 New J. Phys. 11 123019
[50] Radcliffe P, Düsterer S, Azima A, Li W, Plonjes E, Redlin H, Feldhaus J, Nicolosi P, Poletto L and Dardis J 2007 Nucl. Instrum. Methods Phys. Res. A 583 516–25
[51] Andreasson J et al 2014 Opt. Express 22 2497–510
[52] Barty A et al 2008 Nat. Photon. 2 415–9
[53] Mie G 1908 Ann. Phys., Lpz. 330 377–445
[54] Loh N D et al 2012 Nature 486 513–7
[55] Pedersoli E et al 2013 J. Phys. B: At. Mol. Opt. Phys. 46 164033
[56] Zhang G, Wu Z and Li Y 2012 Opt. Express 20 4726–37
[57] Veen F V D and Pfeiffer F 2004 J. Phys.: Condens. Matter. 16 5003–30
[58] Ulanowski Z, Hirst E, Kaye P and Greenaway R 2012 J. Quant. Spectrosc. Radiat. Transfer 113 2457–64
[59] Marchesini S, Chapman H N, London R A and Szoke A 2003 Opt. Express 11 2344–53
[60] DeCastro A, Eremina E, Bostedt C, Hoener M, Thomas H and Möller T 2008 J. Electron Spectrosc. Relat. Phenom. 166–167 21–7
[61] Vartanyants I, Mancuso P, Singer A, Yefanov O M and Gulden J 2010 J. Phys. B: At. Mol. Opt. Phys. 43 194016
[62] Als-Nielsen J 2011 Elements of Modern X-ray Physics (New York: Wiley)
[63] Piederrière Y, Le M J, Cariou J, Abgrall J and Blouch M 2004 Opt. Express 12 4596–601